J Neurophysiol 118: 15–28, 2017.
First published March 15, 2017; doi:10.1152/jn.00278.2016.

RESEARCH ARTICLE | *Sensory Processing*

Visual and presaccadic activity in area 8Ar of the macaque monkey lateral prefrontal cortex

Kelly R. Bullock,[1,4] Florian Pieper,[2] Adam J. Sachs,[3] and Julio C. Martinez-Trujillo[4]

[1]*Department of Physiology, McGill University, Montreal, Quebec, Canada;* [2]*Department of Neurophysiology and Pathophysiology, University Medical Center Hamburg-Eppendorf, Hamburg, Germany;* [3]*Division of Neurosurgery, Department of Surgery, The Ottawa Hospital Research Institute, The University of Ottawa, Ottawa, Ontario, Canada; and* [4]*Robarts Research Institute, Department of Physiology and Pharmacology, Brain and Mind Institute, University of Western Ontario, London, Ontario, Canada*

Submitted 5 April 2016; accepted in final form 8 March 2017

Bullock KR, Pieper F, Sachs AJ, Martinez-Trujillo JC. Visual and presaccadic activity in area 8Ar of the macaque monkey lateral prefrontal cortex. *J Neurophysiol* 118: 15–28, 2017. First published March 15, 2017; doi:10.1152/jn.00278.2016.—Common trends observed in many visual and oculomotor-related cortical areas include retinotopically organized receptive and movement fields exhibiting a Gaussian shape and increasing size with eccentricity. These trends are demonstrated in the frontal eye fields, many visual areas, and the superior colliculus but have not been thoroughly characterized in prearcuate area 8Ar of the prefrontal cortex. This is important since area 8Ar, located anterior to the frontal eye fields, is more cytoarchitectonically similar to prefrontal areas than premotor areas. Here we recorded the responses of 166 neurons in area 8Ar of two male macaques while the animals made visually guided saccades to a peripheral sine-wave grating stimulus positioned at 1 of 40 possible locations (8 angles along 5 eccentricities). To characterize the neurons' receptive and movement fields, we fit a bivariate Gaussian model to the baseline-subtracted average firing rate during stimulus presentation (early and late visual epochs) and before saccade onset (presaccadic epoch). One hundred twenty-one of one hundred sixty-six neurons showed spatially selective visual and presaccadic responses. Of the visually selective neurons, 76% preferred the contralateral visual hemifield, whereas 24% preferred the ipsilateral hemifield. The angular width of visual and movement-related fields scaled positively with increasing eccentricity. Moreover, responses of neurons with visual receptive fields were modulated by target contrast, exhibiting sigmoid tuning curves that resemble those of visual neurons in upstream areas such as MT and V4. Finally, we found that neurons with receptive fields at similar spatial locations were clustered within the area; however, this organization did not appear retinotopic.

NEW & NOTEWORTHY We recorded the responses of neurons in lateral prefrontal area 8Ar of macaques during a visually guided saccade task using multielectrode arrays. Neurons have Gaussian-shaped visual and movement fields in both visual hemifields, with a bias toward the contralateral hemifield. Visual neurons show contrast response functions with sigmoid shapes. Visual neurons tend to cluster at similar locations within the cortical surface; however, this organization does not appear retinotopic.

Address for reprint requests and other correspondence: J. C. Martinez-Trujillo, Western University, Schulich School of Medicine and Dentistry, Dept. of Physiology and Pharmacology, 1151 Richmond St. N, Rm. 7239, London, ON, N6A 5B7 (e-mail: julio.martinez@robarts.ca).

prefrontal cortex; receptive fields; target selection; clustering; saccades

SEVERAL STUDIES have suggested that the lateral prefrontal cortex (LPFC) plays a role in cognitive control of visually guided oculomotor behavior (Barone and Joseph 1989), encoding rules for goal-directed behavior (Miller 1999; Wallis et al. 2001; Wise et al. 1996), adaptive response strategies (Genovesio et al. 2005), attention (Everling et al. 2002; Lennert and Martinez-Trujillo 2011, 2013; Rossi et al. 2007; Tremblay et al. 2015), working memory (Mendoza-Halliday et al. 2014; Miller 1999), decision making (Kiani et al. 2014; Seo et al. 2007), and the ability to suppress automatic behavioral responses (Wegener et al. 2008).

In particular, area 8Ar—the region of the LPFC between the arcuate sulcus and the posterior tip of the principal sulcus (Petrides and Pandya 1999; Preuss and Goldman-Rakic 1991), just anterior to the frontal eye fields (FEF) (Stanton et al. 1989), is a cortical area that likely plays a role in visuomotor integration within the saccade generation network on the basis of its connectivity and response properties. Namely, area 8Ar shares connections with parietal areas responsible for visuospatial processing including areas LIP and 7 (Andersen et al. 1990; Barbas and Mesulam 1981; Petrides and Pandya 1999; Schall et al. 1995b) and is heavily interconnected with the neighboring areas in the LPFC such as area 9/46 and with the FEF (Stanton et al. 1993; Yeterian et al. 2012).

Topography—the orderly projection of sensory receptors onto the cortex—is an organizing principle preserved throughout much of the saccade generation network. For instance, rough retinotopic maps are described in visual areas V4 (Gattass et al. 1988) and MT (Maunsell and van Essen 1983; Ungerleider and Desimone 1986; Van Essen et al. 1981) and frontal areas such as FEF (Bruce et al. 1985; Stanton et al. 1989). Areas of the parietal cortex such as LIP (Arcaro et al. 2011; Ben Hamed et al. 2001; Blatt et al. 1990) are also thought to have topographic organization; however, this issue has not been settled. In addition to retinotopy of visually selective neurons, microstimulation of the FEF in macaques has revealed a topographic organization of saccade amplitude

but not direction (Bruce et al. 1985; Stanton et al. 1989). When stimulated, the dorsomedial portion (in the superior limb of the arcuate sulcus) of FEF produces large-amplitude (15–20°) saccades and the ventrolateral portion (in the inferior limb of the arcuate sulcus) elicits small-amplitude saccades (Bruce et al. 1985). However, it is less clear to what extent the more anterior and superficially located area 8Ar contains a topographic representation of visual and oculomotor space.

Neurons in visual and oculomotor areas respond preferentially to stimuli shown at certain locations in visual space or before saccades toward such locations. This spatially selective firing delineates receptive fields (RFs), the location at which a visual stimulus evokes a firing rate above baseline, and movement fields (MFs), the saccade target location eliciting firing rates above baseline. The baseline is defined as the firing rate when the animal is not engaged in a specific task and visual targets are not present. Suzuki and Azuma (1983) report isocontour lines of RF size and eccentricity within area 8Ar. They found that RF size and eccentricity increase as one moves medially from the inferior arcuate sulcus toward the posterior tip of the principal sulcus. They also observed that RF size, but not eccentricity, increases as one moves anteriorly from the knee of the arcuate sulcus toward the principal sulcus (Suzuki and Azuma 1983). However, these analyses have not been replicated, and to our knowledge no study to date has examined the response properties of RFs and MFs in area 8Ar in detail.

Here we recorded neural responses from the left area 8Ar of two macaques while the subjects performed a visually guided saccade task, using a multielectrode array (MEA). We systematically characterized the RF and MF properties of 8Ar neurons in terms of their spatial extent across eccentricity and contrast sensitivity and investigated the relationship between cortical location and spatial representation. We found that 76% of the recorded neurons preferred the contralateral visual hemifield, whereas 24% preferred the ipsilateral hemifield. Moreover, neurons with RFs and MFs at similar spatial positions were clustered within the same region of the cortical surface.

METHODS

Subjects and ethics statement. All procedures were carried out pursuant to the Canadian Council for Animal Care guidelines and were preapproved by the McGill University Animal Care Committee. Recordings were made from the dorsolateral prefrontal area 8Ar (Petrides and Pandya 1999) of two adult male cynomolgus macaques (*Macaca fascicularis*), henceforth referred to as *monkeys JL* and *F*. Animals were pair-housed in large enclosures; interaction with facility personnel, treats, and toys were provided daily to enrich the environment. On experimental days fluid intake was restricted, and a juice reward was earned by the animals upon successful completion of the task. Water intake was supplemented to guarantee that animals received a minimum of 35 $ml \cdot kg^{-1} \cdot day^{-1}$, even if animals failed to obtain this amount during the experiment. Fresh fruits and vegetables were also provided daily. Animals were monitored for signs of distress or illness. Criteria used to define distress or illness included changes in body weight, grooming habits, and water intake, and these were recorded daily. Other physiological markers of well-being—such as blood cell count, hemoglobin, hematocrit, and kidney function—were examined quarterly. Any indication of discomfort or illness resulted in cessation of the experiment until treatment and recovery were completed, as determined by an animal welfare veterinarian.

Head post and microelectrode array implantation. Before the experiments, three head posts were implanted on each animal: one positioned on the midline posterior to the supraorbital ridge and two placed superior to the external occipital protuberance on the petrosal bones. The head posts allowed for fixation of the animal's head during experimentation.

A 96-channel MEA (4 mm × 4 mm; Blackrock Microsystems) (Maynard et al. 1997; Normann et al. 1999) was implanted in the left dorsolateral prefrontal area 8Ar of each monkey—in the prearcuate gyrus between the posterior end of the principal sulcus and the knee of the arcuate sulcus (Fig. 1*A*), as detailed in Leavitt et al. (2013). Briefly, a craniotomy was made by using a high-powered drill (Anspach) to reveal the principal and arcuate sulci. The dura was opened and the MEA inserted with an array gun (Blackrock Microsystems) to a depth of ~1–1.5 mm from the cortical surface. We performed a duraplasty with synthetic dura (Durepair, Medtronic, Minneapolis, MN) and replaced and secured the bone flap with fixation plates and

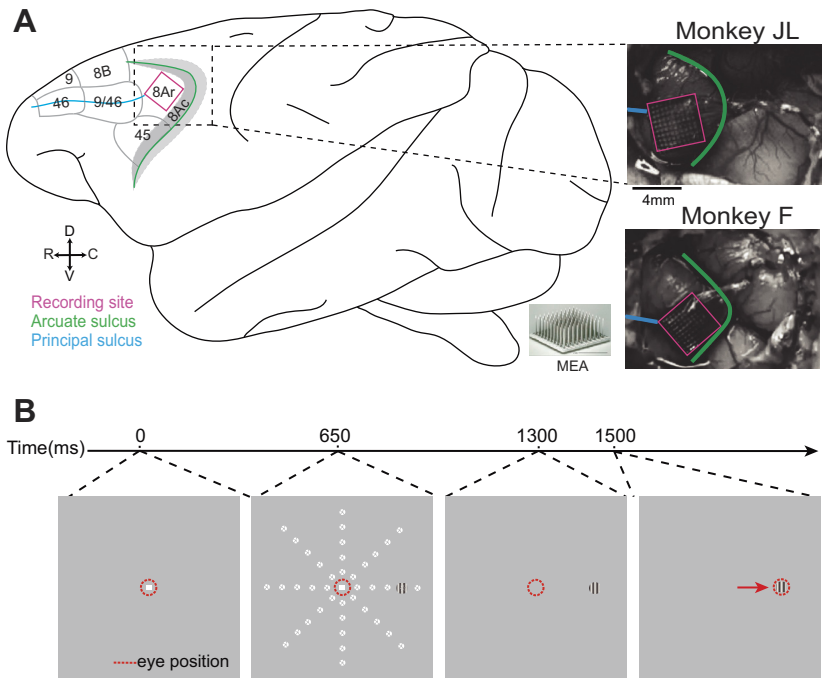

Fig. 1. Recording site and visually guided saccade task. *A*: recording site. A microelectrode array (MEA) was implanted in the left area 8Ar of each monkey, posterior to the posterior end of the principal sulcus and anterior to the arcuate sulcus. Schematic shows cytoarchitectonic delineations of area 8Ar and neighboring prefrontal areas identified by Preuss and Goldman-Rakic (1991) and Yeterian et al. (2012). Photographs show recording site for *monkeys JL* (*top*) and *F* (*bottom*) relative to the sulci labeled in the schematic. C, caudal; D, dorsal; R, rostral; V, ventral. *B*: timeline of visually guided saccade task. After 650 ms of fixation, a peripheral sine-wave grating appears at 1 of 40 locations arranged along 8 polar angles (45° intervals) and 5 eccentricities (3 dva intervals); white dotted circles indicate possible stimulus locations. Monkey maintains central fixation for 650 ms, and at 1,300 ms monkey is cued to saccade to the stimulus upon extinguishing the central fixation point. Monkey receives juice reward upon successfully shifting gaze to target.

screws (Synthes). All surgical procedures were carried out under general anesthesia administered via an endotracheal tube. Animals were fully recovered from surgery within 1 wk.

Data collection. During the experimental session, eye positions were tracked with an infrared eye tracker at a sampling frequency of 500 Hz (EyeLink 1000, SR Research, Ottawa, ON, Canada) (Khayat et al. 2010). The neuronal signal was amplified via a headstage (ICS-96) for a reduced-noise signal, band-pass filtered (0.3 Hz/1 pole, 7.5 kHz/3 pole, analog), and digitized (16 bit, 1 μV/bit, sample rate of 30 kHz) with a neuronal signal processor (Cerebus, Blackrock Microsystems). Spike waveforms were acquired by setting a threshold of -4 to $-4.5\times$ the noise amplitude of the digitized, high-pass filtered raw signal.

For single-unit analysis, individual neurons were isolated based on waveform properties such as peak-to-peak amplitude in principal component space using Offline Sorter (Plexon). The MEA electrodes were evenly spaced along intervals of 0.4 mm and arranged into three blocks of 32 simultaneously recorded electrodes. Each session comprised data collected from one of the three blocks (*A*, *B*, *C*) (Leavitt et al. 2013).

Task. A custom computer program recorded the behavioral data (eye signals and lever presses) and presented the visual stimuli. The screen was positioned 100 cm from the animals' eyes. A trial was initiated when the monkey held gaze position within a 2° window of a central fixation point ($0.08^{\circ 2}$) and pressed a lever to indicate willingness to start the trial. After fixation for 650 ms, a sine-wave grating (2.5 cycles/°, 1° visual angle in diameter, oriented at 90° to the horizontal, luminance contrast of 3%, 5%, 10%, 20%, or 35%) appeared at 1 of 40 randomly selected locations, arranged along eight polar angles in steps of 45° and five eccentricities spaced in increments of 3 degrees visual angle (dva) (Fig. 1*B*). The monkey maintained central fixation for 650 ms of stimulus presentation, after which the central fixation point was extinguished, cuing the monkey to saccade to the peripheral stimulus. If the monkey initiated the saccade within 125–600 ms of the response cue, and the saccade end point landed within a radius of 1.25 dva of the stimulus, a juice reward was given. Fixation breaks, premature lever releases, or failing to land on the saccade target resulted in a failed trial, which was aborted without reward.

Data analysis. All data analysis was conducted with MATLAB software (MathWorks, Natick, MA). Spike waveforms were stored as discreet spike event times (the nearest millisecond following threshold crossing). For single-cell analysis, we recorded from a total of 166 neurons (60 in *monkey JL*; 106 in *monkey F*) across three sessions for each subject. In each session, we recorded from a block of 32 channels designated as *blocks A*, *B*, and *C*, which together comprise an entire array. For *monkey JL* we isolated neurons from *blocks A*, *B*, and *C*, and in *monkey F* we isolated neurons from two sessions in *block B* and one from *block C*. Any isolated neurons with a maximum firing rate of <1 spike/s were excluded from analysis. For topographic analysis, we used the thresholded signal on the electrodes from *blocks A*, *B*, and *C* for both animals in order to maximize the number of electrodes included in the analysis.

For single-cell RF and MF analysis, to ensure sufficient trial numbers, we pooled across trials with the highest contrast levels (10%, 20%, and 35% contrast) and measured the average visual and movement activity of area 8Ar neurons during the early visual (duration 250 ms; 100 ms after stimulus onset), late visual (duration 250 ms; 350 ms after stimulus onset), and presaccadic (duration 100 ms; immediately before saccade onset) epochs and the baseline firing rate (duration 250 ms; 250 ms after trial initiation) (see Fig. 3*B*). We divided the visual epoch into early visual and late visual periods to account for temporal dynamics of the visual response. The peristimulus time histogram was computed across an average of 18 trials (SD = 7) in 50-ms bins.

Saccade precision and kinematics. We recorded the monkeys' eye position and calculated the duration of the saccade: from the time at which the eye (gaze) velocity exceeded the threshold of 25°/s to when it returned to that threshold. Peak velocity was considered to be the maximal velocity during a saccade. Saccade end-point location was determined as the eye position when eye movement velocity returned to the saccadic velocity threshold. To quantify saccade precision we measured the area covered by clusters of saccade end points around a target; only saccade end points from hit trials were included in the analysis. An ellipse was fit to the cluster of saccade end points to a given target with the least-squares method, and its area was computed as a measurement of saccade end-point spread (Fig. 2*C*).

Receptive and movement fields. To determine whether RF and MF width scales with eccentricity, we plotted the tuning curve at each eccentricity for the RFs (visual epochs) and MFs (presaccadic epoch). To obtain the tuning curve at each eccentricity, we fit a Gaussian function (*Eq. 1*) to the activity as a function of the angle $f(x)$, using the nonlinear least-squares method:

$$f(x) = a + b \times e^{-\frac{1}{2}\times\left(\frac{x-\mu}{\sigma}\right)^2} \quad (1)$$

where a is the baseline or intercept, b is the height or amplitude of the peak, σ is the standard deviation, and μ is the mean. To minimize error in the Gaussian model fits and to account for the circular nature of the data, tuning curves were centered on the peak or maximal response. The tuning width for a given eccentricity was determined from the standard deviation of the corresponding Gaussian function. The RF and MF width at each eccentricity (r, in dva) was considered to be the arc length (s, given in dva) subtended by the angular width of tuning (θ, in degrees) (*Eq 2*).

$$s = r \times \theta \quad (2)$$

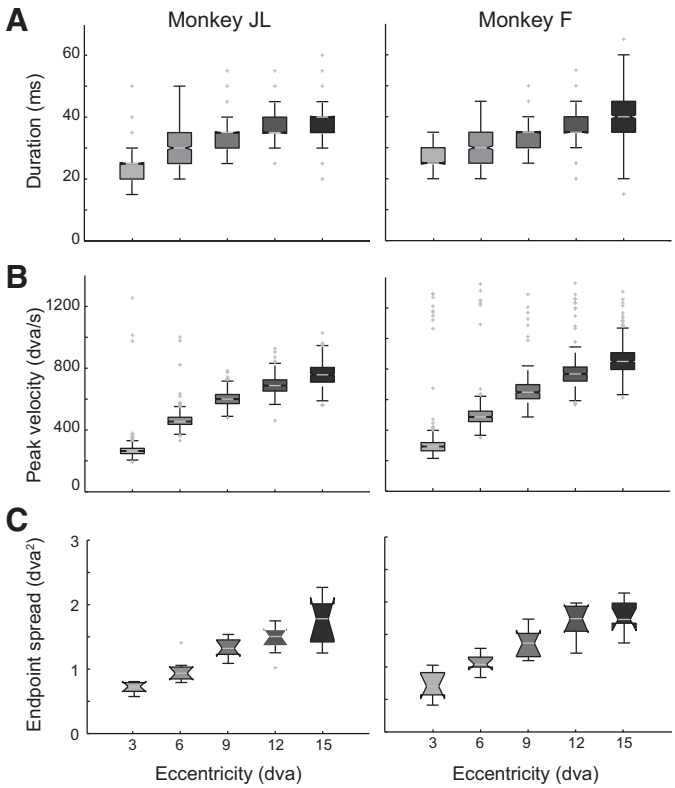

Fig. 2. Saccade kinematics and saccade precision for *monkeys JL* (*left*) and *F* (*right*). Only saccade end points from hit trials are included. *A*: saccade duration as a function of eccentricity. Duration was calculated from the eye velocity trace as the time from when the velocity first exceeded the threshold (25°/s) to when it returned to threshold. *B*: saccade peak velocity as a function of eccentricity. *C*: saccade end-point spread as a function of eccentricity. The spread of the saccade end-point clusters is derived from the area of the ellipse fit to the cluster of end points at each target location.

To assess the spatial extent and location of the RFs (comprising early and late visual epochs) and MFs (presaccadic epoch), a two-dimensional Gaussian function was fit to the baseline-subtracted average activity at the 40 locations, and values between stimulus locations were interpolated (linear interpolation):

$$f(x,y) = a + b \times e^{-\frac{1}{2-\rho}\times\left[\left(\frac{x-\mu_x}{\sigma_x}\right)+\left(\frac{x-\mu_y}{\sigma_y}\right)-\left(\frac{2\times\rho\times(x-\mu_x)\times(y-\mu_y)}{\sigma_x\times\sigma_y}\right)\right]} \quad (3)$$

where $f(x, y)$ is the response at location (x, y), a is the intercept, b is the amplitude, ρ is the correlation between x and y, and μ_x, μ_y, σ_x, σ_y are the mean and variance/width along the Gaussian in the x- and y-axes, respectively. The peak of the Gaussian indicates the preferred location of a given neuron. Neurons were considered tuned for a given epoch if activity at one location was significantly modulated (Kruskal-Wallis test, $P < 0.05$) with a goodness of fit (R^2) > 0.75 for the Gaussian model (as per Hair et al. 2012). Some units exhibited activity at one or more locations that was vigorously suppressed below baseline. We categorized any unit with suppression of at least 50% the magnitude of the peak activation of that cell as a "suppressed cell." We only considered selective neurons ($n = 121$) in our single-cell RF and MF analysis.

Contrast response functions. Visual neurons in the macaque LGN as well as areas V1 and MT have demonstrated a saturating relationship between the neural response and increasing stimulus contrast (Albrecht and Hamilton 1982; Sclar et al. 1990). However, it is still unclear how contrast is encoded in LPFC area 8Ar. We examined the response of 7 visual (tuned in early visual epoch; Kruskal-Wallis test, $P < 0.05$), 61 visuomovement (tuned in early visual and presaccadic epochs; Kruskal-Wallis test, $P < 0.05$), and 7 movement (tuned in presaccadic epoch; Kruskal-Wallis test, $P < 0.05$) neurons in response to stimuli of 3%, 5%, 10%, 20%, and 35% contrast [contrast = $\Delta L/L_{min}$, where ΔL is the maximum luminance minus the minimum luminance (L_{min})] (Michelson 1927). We included in the analysis only cells for which there were at least three trials presented at each contrast level and exhibiting a maximum firing rate across all contrast of at least 5 spikes/s. We first subtracted the baseline firing rate to determine how contrast modulates activity relative to baseline. We then fit a sigmoid function to the contrast response:

$$R = \frac{R_{max} \times C^n}{C^n + C_{50}^n} + M \quad (4)$$

where R_{max} refers to the difference in firing rate between response at saturation and response at lowest contrast level (M). C_{50} represents the contrast at which the activity is at half saturation, and n is the slope of the sigmoid function (Martínez-Trujillo and Treue 2002). We included only cells with a goodness of fit (R^2) > 0.7 (Hair et al. 2012).

Response latencies. Previous studies have observed that the distribution of interspike intervals in a spike train can be modeled by the Poisson distribution (Hanes et al. 1995). Poisson spike train analysis can therefore determine periods of significant neuronal activation by comparing the observed number of spikes within a given interval to the number that would be predicted if the spikes followed a Poisson distribution (the null hypothesis).

Using this analysis method, we computed a surprise index (SI), which acts as a metric of the improbability that a burst of neural activity occurs by chance. The SI is computed thus:

$$SI = -\log P \quad (5)$$

where P is the probability of a Poisson-distributed (random) spike train. The Poisson formula is as follows:

$$P = e^{-rT}\sum_{i=n}^{\infty}(rT)^i/i! \quad (6)$$

where P is the probability that a spike train with a mean firing rate (r) will contain n or more spikes in the time interval (T) (Hanes et al. 1995).

Clustering. We assessed whether the preferred location (in Cartesian coordinates) of the neurons on a given electrode displayed nonrandom spatial organization on the cortex. The preferred location on a given channel was defined by the location of the peak of the bivariate Gaussian fit to the baseline-subtracted thresholded activity on an electrode. We examined the coefficient of determination (R^2) as a metric of goodness of fit. Only electrodes with an acceptable goodness of fit ($R^2 > 0.5$) were considered for clustering analysis.

To determine whether similar preferred locations were anatomically clustered, we utilized Moran's I, a measure of spatial autocorrelation (Moran 1950; Zuur et al. 2007). Moran's I is defined as

$$I = \frac{N}{\sum i \sum j \omega ij}\frac{\sum i \sum j \omega ij\left(X_i - \overline{X}\right)\left(X_j - \overline{X}\right)}{\sum i\left(X_i - \overline{X}\right)^2} \quad (7)$$

where N is the number of spatial units as indexed by i and j, X is the variable of interest, $\overline{X}$ is the mean of X, and ωij is an element of a matrix of spatial weights. Moran's I ranges from -1 to $+1$, with negative values indicating that channels with similar values are maximally mutually separated and positive values indicative that similar values occupy neighboring electrodes. A value of 0 indicates a random spatial relationship of values on the array.

RESULTS

We recorded the activity of 166 neurons in the left area 8Ar of two macaque monkeys. The animals correctly learned and performed the task. The performance was higher than 95% in all sessions (3 sessions per subject).

Saccade kinematics and precision. Saccades made by the animals follow stereotypical kinematics rules, namely, the duration and peak (maximal) velocity of saccades scale as a function of saccade amplitude, thus following the main sequence (Bahill et al. 1975). Figure 2 shows the data from *monkeys JL* and *F*. We plotted the saccade duration (Fig. 2*A*) and saccade peak velocity (Fig. 2*B*) as a function of eccentricity; both animals displayed very similar saccade kinematics. Both the mean saccade duration (Fig. 2*A*) and peak velocity (Fig. 2*B*) displayed a monotonic positive scaling with eccentricity. The saccade end-point spread, a measure of saccadic precision, was determined at various eccentricities from the area of ellipses fit to saccade landing position clusters around the target center position. The area of saccade-end point clusters monotonically increased as a function of eccentricity (Fig. 2*C*), in agreement with previous studies (Kowler and Blaser 1995).

Visual and movement response properties. We isolated the responses of 166 neurons (60 in *monkey F* and 106 in *monkey JL*) during the different periods of the task. Figure 3*A* shows the peristimulus time histograms (50-ms time bins) of an example neuron's (*FS2C12U2*) activity corresponding to the 40 stimulus locations. In line with previous studies, we observed different visual response profiles among single cells (Fig. 3, *C–F*) (Mikami et al. 1982; Suzuki and Azuma 1983): phasic activation, tonic activation, phasic-tonic activation, and tonic suppression. We divided the visual period—during which the monkey fixated while a peripheral stimulus ap-

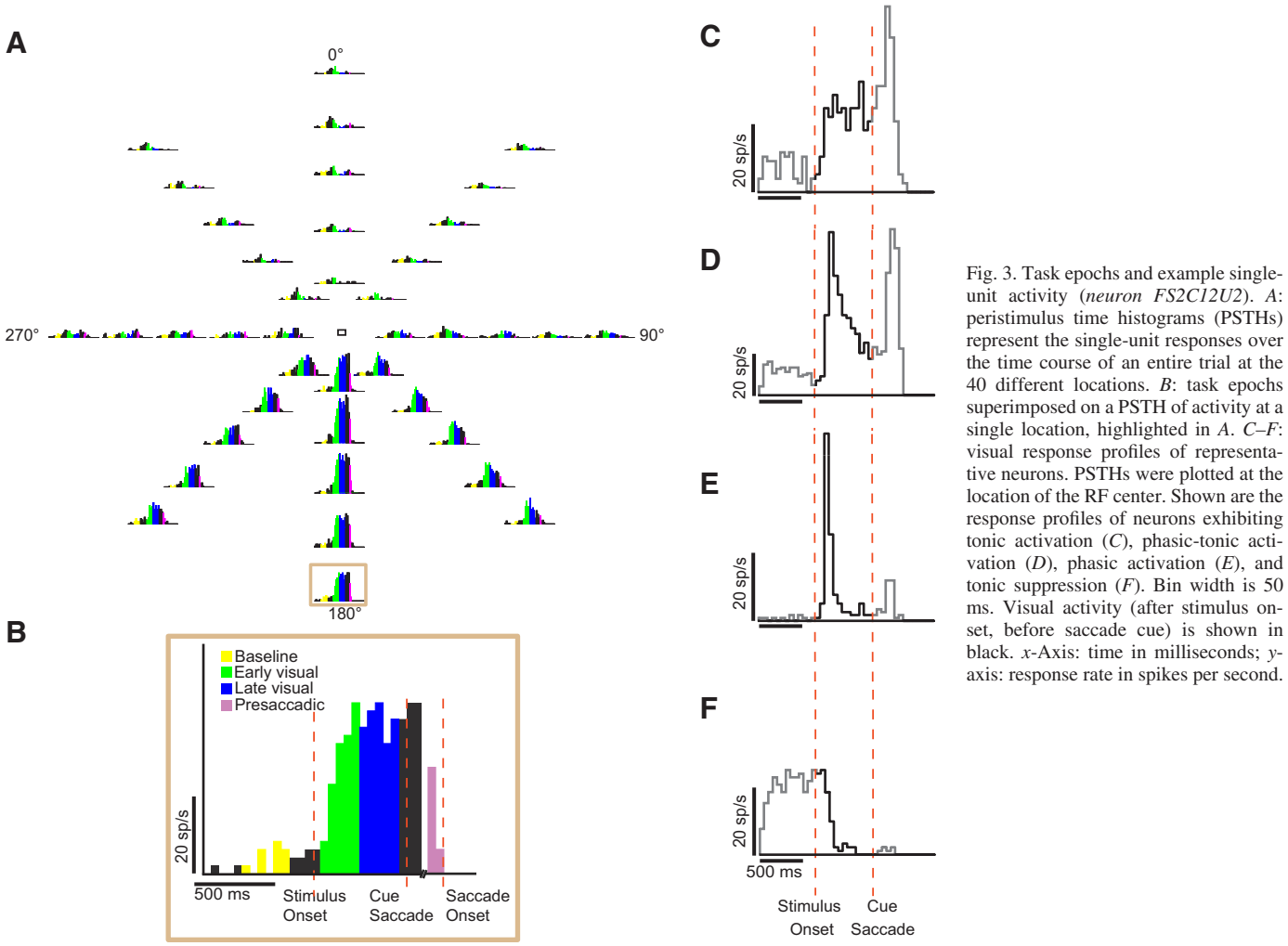

Fig. 3. Task epochs and example single-unit activity (*neuron FS2C12U2*). *A*: peristimulus time histograms (PSTHs) represent the single-unit responses over the time course of an entire trial at the 40 different locations. *B*: task epochs superimposed on a PSTH of activity at a single location, highlighted in *A*. *C–F*: visual response profiles of representative neurons. PSTHs were plotted at the location of the RF center. Shown are the response profiles of neurons exhibiting tonic activation (*C*), phasic-tonic activation (*D*), phasic activation (*E*), and tonic suppression (*F*). Bin width is 50 ms. Visual activity (after stimulus onset, before saccade cue) is shown in black. *x*-Axis: time in milliseconds; *y*-axis: response rate in spikes per second.

peared—into "early visual" and "late visual" epochs to account for the temporal dynamics of the visual response and to ensure that the visual time window was similar to that for the presaccadic epoch (colors in Fig. 3*B* delineate epochs).

Because of its extensive connections with visual and oculomotor areas within the saccade generation circuit, area 8Ar likely plays a role in visuomotor integration and preparation of saccades. One of our goals was to determine whether the neurons' RFs and MFs exhibit a Gaussian shape and scale with eccentricity, a trend observed in other visual (Schall 1995) and oculomotor (Sparks et al. 1976) areas. We plotted tuning curves—the mean activity across polar angle—for each eccentricity (Fig. 4*A*). We then determined the angular width of tuning from twice the standard deviation of a univariate Gaussian to the peak-centered tuning curve at each eccentricity (Fig. 4*A*, *inset*). Figure 4*B* shows that RF and MF width scale positively as a function of eccentricity (Kruskal-Wallis test, $P < 0.05$).

It has been reported that RFs in area 8Ar tend to be large—ranging from 10 × 10 to 60 × 60 dva (Mikami et al. 1982)—and show a bias for the contralateral visual hemifield (Suzuki and Azuma 1983). Figure 5*A* shows the RFs measured during the early and late epochs of visual stimulation and the MF of two example neurons. The spatial extent of both fields was very similar. We estimated the RF and MF centers from the Cartesian coordinates of the peak of the bivariate Gaussian fit to the activity. We followed the same procedure for all 166 of the recorded neurons. We excluded 45 (27%) of the 166 single units that failed to demonstrate significant response modulation compared with baseline in any of the epochs (Fig. 5*B*). Of the neurons that were tuned ($n = 121$, Kruskal-Wallis test, $P < 0.05$), 68 (56%) were visuomovement cells (tuned in either early visual or late visual and presaccadic epochs); 39 (32%) were visual cells (tuned in either early or late visual epoch); and 14 (12%) were movement cells (tuned in the presaccadic epoch only) (Fig. 5*B*). Of the cells that were visually selective (including visual and visuomovement cells, $n = 107$), 81 (76%) preferred the contralateral visual hemifield, that is, the peak of the Gaussian defining the RF center was contralateral to the recording site. By contrast, only 26 (24%) of the units preferred the ipsilateral hemifield (Fig. 5*C*). This bilateral representation with a contralateral bias agrees with previous studies reporting 42% ipsilateral and 58% contralateral preference in the LPFC (Lennert and Martinez-Trujillo 2013). Movement neurons also displayed a preference for the contralateral hemifield, with 10/13 (77%) of MFs in the contralateral hemifield compared with 3/13 (23%) in the ipsilateral hemifield (Fig. 5*D*) and 1 that lay on the meridian.

Suppression below baseline. Whereas most cells exhibited only elevated response in their RF and MF, a subset ($n = 15$)

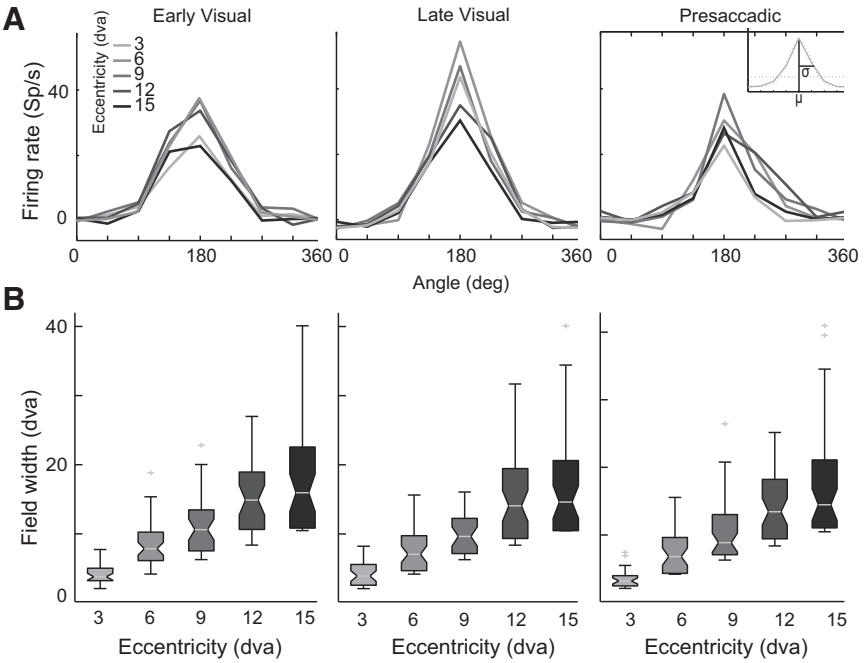

Fig. 4. Width of tuning across eccentricities. *A*: single-neuron (*FS2C12U2*) tuning curves for each eccentricity plotted for the different task epochs: early visual (*left*), late visual (*center*), and presaccadic (*right*). *Inset*: a univariate Gaussian fit to the tuning curve for each eccentricity. The angular width of tuning is determined from the standard deviation (σ) of the Gaussian model at each eccentricity. *B*: population receptive and movement field width as a function of eccentricity. Fill colors correspond to the eccentricities depicted in *A*.

of visually selective cells had zones of suppression relative to baseline as well as zones of activation above baseline within their RF (Fig. 5*A*, *bottom*). We considered a cell to be suppressed if the magnitude of suppression was at least 50% of the peak activation of that cell. We characterized cells exhibiting only activation as nonsuppressed. The characterization of suppressed cells is such that cells with a low baseline firing rate may not be considered suppressed, as the magnitude of suppression is inevitably limited by the baseline activity. For our purposes, a neuron's "preference" was considered the location of peak activation above baseline, for both suppressed and nonsuppressed neurons. For suppressed cells, the zone of suppression was invariably in the antipreferred location of the cell. Our conservative criteria may underestimate the proportion of suppressed cells; it was intended to avoid false positives.

There was a strong bias for representing the contralateral visual hemifield among nonsuppressed cells (Fig. 5*C*). However, a significantly higher proportion (z score, $P < 0.05$) of suppressed cells preferred the ipsilateral hemifield (9/15; 60%) compared with the proportion of nonsuppressed cells preferring the ipsilateral hemifield (17/92; 18%) (Fig. 5*C*). Conversely, only 6/15 (40%) of suppressed cells compared with 75/92 (82%) of nonsuppressed preferred the contralateral hemifield. Therefore, suppressed cells tended to have a stronger preference for the ipsilateral hemifield compared with nonsuppressed cells.

Receptive field-movement field overlap. We examined whether the RF and the MF of the visuomovement neurons overlap. To this end, we determined the center of the RF (early visual epoch) and MF (presaccadic epoch) and computed the Euclidean distances between them for 17 cells in *monkey JL* and 30 cells in *monkey F*. We found that for most cells the RF and MF centers were located within 4 dva of each other (Fig. 6*A*). However, in some neurons, particularly in *monkey F*, the field shifted by >10 dva from the early visual to the presaccadic epoch. This suggests that in some recorded neurons a complex transformation from visual signals into motor commands may take place.

We also compared the size of the RF and MF. We calculated the elliptical area of the bivariate Gaussian model from the standard deviation along the minor and major axes. There was a significant positive correlation between RF and MF size for the visuomovement neurons of both *monkeys JL* and *F* (Pearson's correlation, $P < 0.05$) (Fig. 6*B*). There was a tendency, particularly in *monkey F*, for the MFs to be slightly larger. We examined whether difference in size was correlated with the magnitude of the field shift and found a poor correlation between the two variables, with a weak correlation in *monkey F* (Pearson's correlation, $P < 0.05$) and a nonsignificant correlation in *monkey JL* (Fig. 6*C*). Our relatively small sample size makes interpretation of these results difficult. Therefore, this question needs to be addressed with a larger sample size in future studies.

Contrast response functions. Whereas the relationship between contrast level and visual response has been thoroughly described in early visual areas, fewer studies have elucidated how contrast is encoded in higher cortical areas, and to our knowledge none has addressed this question in area 8Ar. We examined the contrast response function in representative visual, visuomovement, and movement cells (Fig. 7*A*). As anticipated, visual and visuomovement (but not movement) cells exhibited a sigmoidal relationship between neural response and contrast level in the early visual epoch with no modulation of response as a function of contrast during the presaccadic epoch. We determined that 19 of 67 (28.4%) visually selective cells in *monkey F* and 14 of 40 (35.0%) in *monkey JL* were modulated by contrast ($R^2 > 0.7$) in the early visual epoch (Table 1). From these best-fit models of sigmoid function, we determined the distribution of parameters for the contrast response functions of visually selective cells in area 8Ar (Fig. 7*B*). Cells demonstrated a median R_{max} of 18.0 for *monkey F* and 20.8 for *monkey JL*; exponent (n) of 2.9 for *monkey F* and 3.1 for

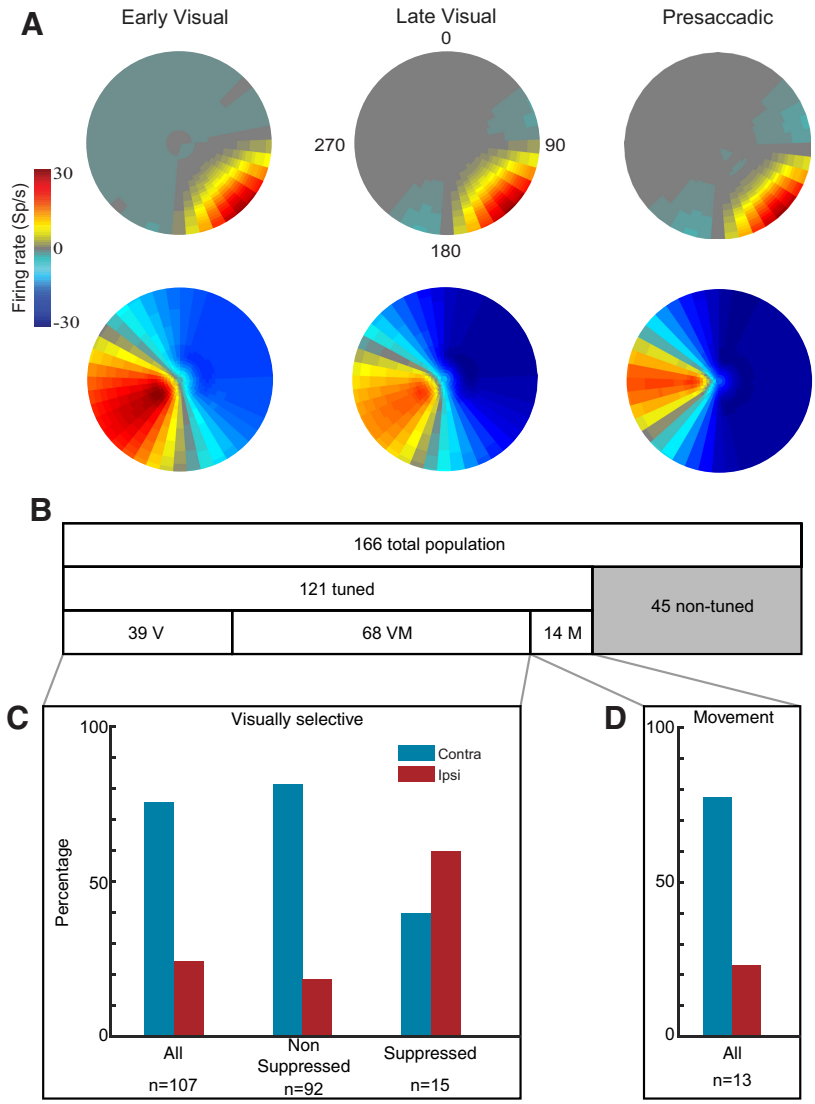

Fig. 5. Receptive and movement fields. *A*: receptive fields (RFs; early and late visual epochs) and movement fields (MFs; presaccadic epoch) for example nonsuppressed neuron (*top*) and suppressed neuron (*bottom*). A 2-dimensional Gaussian is fit to the mean baseline-subtracted activity at the 40 locations; values between stimulus locations are interpolated. Firing rate relative to baseline represented by color bar. *B*: population visuomotor tuning. Horizontal bars show the proportion of visual (V), visuomovement (VM), and movement (M) neurons. Tuned neurons refer to the proportion of neurons with significant task-related activity (ANOVA, $P < 0.05$). Gray section represents the proportion of neurons without selectivity during any of the task epochs. *C*: % of neurons with preferred locations in the contralateral compared with the ipsilateral visual hemifield among all visually selective—visual and visuomovement—neurons (*left*), nonsuppressed neurons (*center*), and suppressed neurons (*right*). *D*: % of movement neurons preferring the ipsilateral (red) and contralateral (blue) hemifield.

monkey JL; semisaturation constant (C_{50}) of 5.6 for *monkey F* and 3.9 for *monkey JL*; and a minimum-contrast response (M) of −1.4 for *monkey F* and −1.8 for *monkey JL* (Table 1). The parameter distributions were the same between individuals, save for the C_{50}, which was lower in *monkey JL* (Table 1; Wilcoxon rank sum, $P < 0.05$). This may reflect individual differences in contrast sensitivity between the two animals. We also examined response latency of contrast-modulated cells ($n = 33$) using Poisson spike train analysis (as detailed in Hanes et al. 1995; Legéndy and Salcman 1985) and plotted these latencies as a function of contrast (Fig. 8). We found that the response latency decreases monotonically as a function of contrast.

Topographic organization of location preference. A hallmark study into the systematic anatomical organization of RF size and eccentricity in the LPFC revealed isocontour lines of these neuronal RF features in the region between the arcuate sulcus and the posterior tip of the principal sulcus (Suzuki and Azuma 1983). Although the systematic organization of unidimensional variables (eccentricity or angle) has been queried, anatomical clustering according to the two-dimensional preferred location has not been described.

The preferred location of an electrode on the array was mapped onto its cortical position according to a two-dimensional spatial color map (Fig. 9*C*). Space was discretized into five eccentricities and four quadrants. Moran's I (spatial autocorrelation) was computed over every unique distance between elements on the array, considering first only the nearest neighbors and increasing the spatial scale until the entire array was considered. Comparisons of location selectivity on a single electrode with itself (distances of 0) were excluded. Chance values were obtained via permutation test. We randomly shuffled each electrode's spatial preference label (excluding the nontuned electrodes) 1,000 times, taking the 95 percentile range of chance values (Fig. 9*B*, gray shaded region) for comparison with our experimental Moran's I values. The analysis of Moran's I revealed clusters of similar location preference on the cortex up to a spatial scale of 4 mm for *monkey JL* and 1.5 mm for *monkey F* (Fig. 9*B*).

We also analyzed the degree of clustering of neurons according to their preferred angle and eccentricity. We mapped the preferred angle (discretized into quadrants) and the preferred eccentricities onto the arrays according to the respective spatial color maps (Fig. 10*C*) and applied Moran's I analysis to

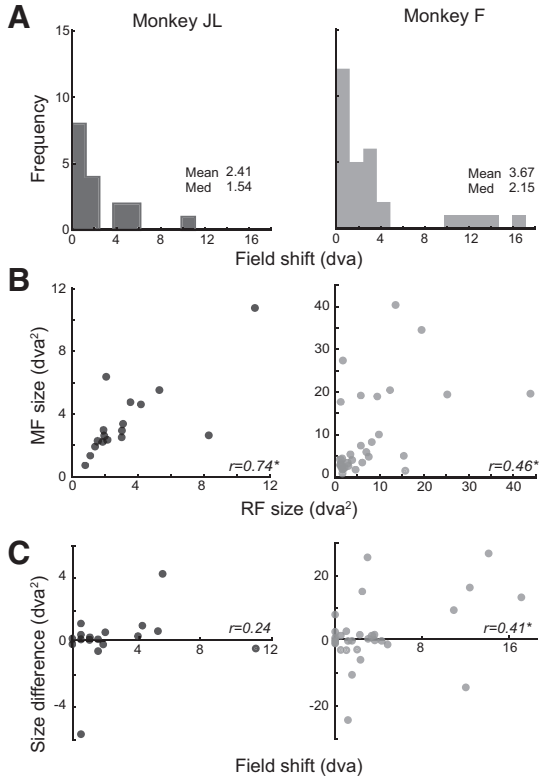

Fig. 6. Receptive and movement field overlap. *A*: distribution of field shifts from receptive field (RF) to movement field (MF). The magnitude of the field shift was given by the Euclidean distance (in dva) between the center of the RF and MF of each visuomovement neuron in *monkeys JL* (*left*) and *F* (*right*). *B*: correlation between RF and MF size. Size was determined as the area of the elliptical perimeter of the 2-dimensional Gaussian. Pearson's correlation (r) reported at *bottom right*; significant ($P < 0.05$) correlations denoted with an asterisk. *C*: correlation between field size difference and field shift. The difference in size ($MF_{area} - RF_{area}$) is plotted against the magnitude of the field shift.

determine the degree of clustering according to these spatial dimensions. *Monkey F* did not show any clustering according to angle or eccentricity (Fig. 10*B*). For *monkey JL*, however, we found that neurons with similar angular preference were clustered between 1 and 4 mm for the early visual epoch and up to 4 mm for the late visual and presaccadic task epochs (Fig. 10*B*). Taken together, the topographic analysis suggests that neurons with RFs and MFs in similar locations were clustered on the cortical surface.

DISCUSSION

We showed that area 8Ar of the LPFC contains spatial representations of both visual hemifields, although biased toward the contralateral visual hemifield. These representations comprise populations of neurons with visual, movement, and visuomovement activity. Neurons within the area have Gaussian-shaped RFs and MFs that scale with eccentricity. The responses of visual and visuomovement neurons are modulated by stimulus contrast. We also observed that neurons with RFs in the ipsilateral hemifield tend to exhibit activity suppressed below baseline when a stimulus is presented in locations opposite to their excitatory RFs. Finally, although area 8Ar receives a multitude of inputs (Yeterian et al. 2012) from retinotopically organized cortical areas—including area MT and V4 (Felleman and Van Essen 1991)—our results do not support the notion that area 8Ar is retinotopic. However, we found clusters of neurons with similar RF locations in both animals during the early period of the visual response.

Response properties of neurons in area 8Ar. Several response profiles have been reported in area 8Ar neuronal populations, including phasic activation, tonic activation, phasic-tonic activation, and tonic suppression (Mikami et al. 1982; Suzuki and Azuma 1983). Phasic activation is characterized by a brief surge of discharge shortly (~100 ms) after the appearance of the visual stimulus, after which activity returns to baseline within 750 ms (Mikami et al. 1982). Cells exhibiting tonic activation, however, increase their firing rate and maintain it until the stimulus is removed. Phasic-tonic activation is characterized by a transient surge in firing rate followed by steady discharge lasting the duration of the visual stimulus. Tonic suppression below baseline is apparent in some cells with high baseline firing rate during fixation and maintains suppression as long as the visual stimulus is presented. In the present study, we observed examples of each of these response profiles (Fig. 3, *C–F*).

It is known that the spatial resolution of vision becomes increasingly coarse moving from the fovea toward the periphery (Schall 1995; Spillmann et al. 1987). One proxy for the decrease in visual acuity toward the periphery is the relationship between RF size and eccentricity, as these two factors have been found to vary systematically and inversely as a function of distance from the fovea across many visual areas (Hubel and Wiesel 1974; but see Dow et al. 1981). This trend results from the high foveal receptor density in the retina and a gradient drop-off toward the margins. Moreover, because fewer neurons are devoted to representing the visual peripheral, eccentric RFs are larger. Indeed, a positive relationship between RF size and eccentricity has been demonstrated in area V1 (Van Essen et al. 1984). Cortical magnification is greater in V1 compared with area 8Ar (present study); this is reflected in the fact that the small, parafoveal RFs in V1—which range from 0.25° to 0.75° in diameter (Hubel and Wiesel 1968)—are much smaller than the width of RFs near the fovea in area 8Ar (ranging from ~2° to 7°) (present study, Fig. 4*B*).

We observed large RFs whose width scales with eccentricity (Fig. 4). In contrast to the smaller, Gaussian RFs in early visual areas, RFs of area 8Ar neurons tend to be elongated and extend across multiple eccentricities. It is possible that RF shapes in this area are more complex than reported here; with our mapping stimulus, it is difficult to estimate the exact shape of these RFs (e.g., deviation from a Gaussian shape or the existence of multiple excitatory and inhibitory fields). In interpreting Gaussian fits one must take into account the sampling resolution of the current method. The Gaussian model estimated the peripheral boundaries with less certainty than at more foveal locations, because the probe resolution decreases in the periphery. This occurs as a trade-off between sampling resolution and the parameters tested, such as location and contrast level. Sampling resolution in the periphery was reduced in order to ensure enough trials for each condition (40 locations with 5 contrast levels). This sampling method guarantees sufficient trials for the analysis of neuronal responses but has the disadvantage of a nonhomogeneous sampling of eccentricities.

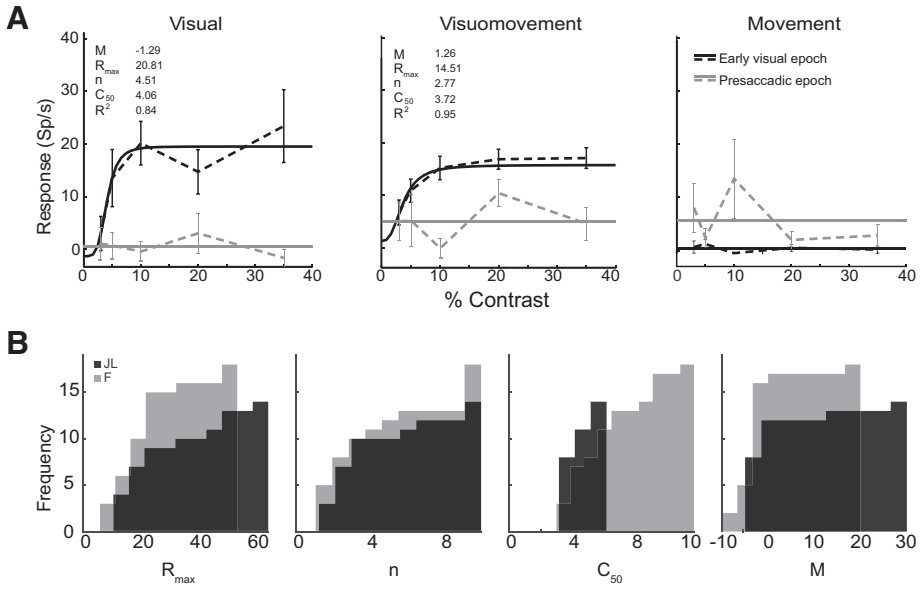

Fig. 7. Contrast response functions. *A*: mean response relative to baseline depicted for example visual (*left*), visuomovement (*center*), and movement (*right*) neurons during the early visual and presaccadic epochs at the location of peak activity. Dashed lines connect mean firing rate for each contrast level, and solid lines represent the best-fit function (either a sigmoid function if $R^2 > 0.7$ or a line through the mean activity); error bars depict SE across all trials presented at that contrast level. *Insets*: parameter values for the sigmoid function fit to the data as well as the goodness of fit (R^2). *B*: parameter values for contrast response functions of visually selective cells. Cumulative distributions of parameters (R_{max}, n, C_{50}, M) for *monkeys F* and *JL* are shown. The optimized parameters were determined by the sigmoid model fits ($R^2 > 0.7$).

One issue that makes it difficult to fully characterize the RF profiles of these neurons is that RFs in this area can change dynamically under different conditions. For example, RFs in extrastriate, parietal, and prefrontal areas such as MT (Womelsdorf et al. 2008), V4 (Tolias et al. 2001), LIP (Ben Hamed et al. 2001), and the LPFC (Lennert and Martinez-Trujillo 2013) have been shown to change depending on task type. In the present study, we have used a limited set of stimuli and a relatively simple task; thus our results in terms of RF and MF profiles may change under different task conditions.

We categorized neurons according to their visual, movement, and visuomovement activity. Visual cells are considered those with significant activity in response to visual stimuli but not preceding a saccade; movement cells discharge immediately preceding a saccade; and visuomovement cells discharge in response to visual stimuli as well as immediately preceding a saccade, according to the criteria established by Bruce and Goldberg (1985). We focused on presaccadic activity, as opposed to postsaccadic activity, as we were interested in the signal preceding saccade execution, which may contribute to saccade planning. We found that, of the 166 isolated neurons, 45 (27%) did not respond to the stimulus or in preparation for a saccade. Of the cells exhibiting significant modulation ($n = 121$), we found 68 (56%) visuomovement neurons, 39 (32%) visual neurons, and 14 (12%) movement neurons (Fig. 5*B*). These results are in agreement with those of Takeda and Funahashi (2002), who recorded from single neurons within the periprincipal region of the LPFC, rostral to area 8Ar, during an oculomotor delayed-response task. They found that 86% of neurons encoded visual stimulus location (visual cells) and 13% encoded the saccade location (movement cells). Although the exact proportion of cells with visual, movement, or visuomovement tuning is difficult to determine with single-cell recordings, because of sampling bias, these studies strongly suggest that visuomovement cells are the most frequently encountered type, followed by visual and movement cells.

Table 1. *Median parameter values of contrast response functions fit to activity of contrast-modulated neurons*

Monkey	No. of Units	R_{max}	n	C_{50}*	M
JL	14	20.8	3.1	3.9	−1.8
F	19	18.0	2.9	5.7	−1.4

*Significantly different between *monkeys JL* and *F* (Wilcoxon rank sum, $P < 0.05$).

Hemifield representation bias. A bias for representation of the contralateral hemifield in saccade-related and visual activity is common among many visual and oculomotor areas. For example, presaccadic neurons within the FEF overwhelmingly prefer saccades toward the contralateral hemifield (Bruce and Goldberg 1985). Indeed, a bias has been reported for contraversive saccades among saccade-related neurons in LIP (Patel et al. 2010), in the SEF (Schlag and Schlag-Rey 1987), in the superior colliculus (Sparks and Mays 1980), and in the periprincipalis region of the LPFC (Funahashi et al. 1991).

In the present study, we found that 81 (76%) of visually selective cells ($n = 107$) preferred the contralateral hemifield, compared with 26 (24%) ipsilaterally preferring cells (Fig. 5*C*). Lennert and Martinez-Trujillo (2013) sampled populations of neurons in area 8Ar and in the anteriorly adjacent area 9/46 and observed a proportion of 58% neurons preferring contralateral and 42% preferring ipsilateral visual targets, indicating that as one moves rostrally within the LPFC the representation of the

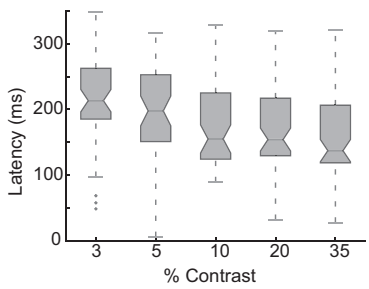

Fig. 8. Visual response latency as a function of contrast levels. Box plots represent the visual response latencies of all contrast-modulated neurons ($n = 33$) from both subjects as a function of contrast level. The visual response latency relative to stimulus onset was calculated with Poisson spike train analysis applied to all trials at each contrast level.

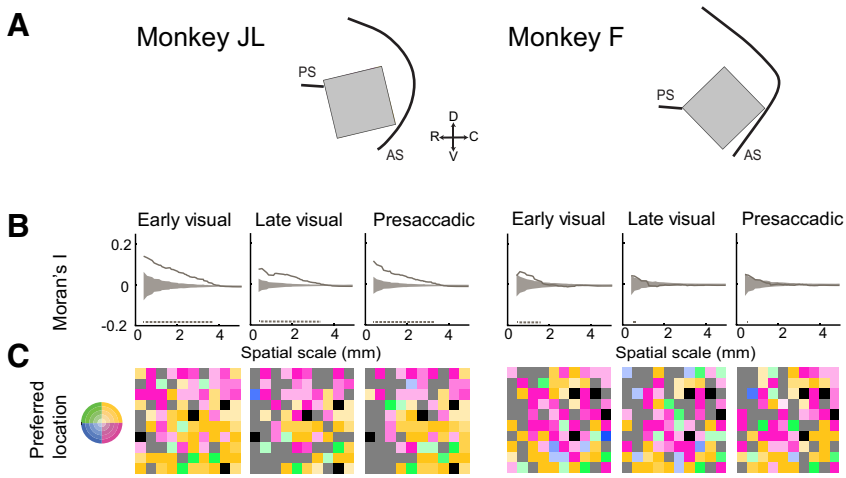

Fig. 9. Anatomical clustering of preferred location across task epochs. *A*: schematic illustrating position of array implants in *monkeys JL* (*left*) and *F* (*right*) relative to the principal (PS) and arcuate (AS) sulci. For *C*, arrays shown in *A* are rotated clockwise until parallel to the horizontal. *B*: magnitude of clustering of preferred location. Solid gray line depicts the spatial autocorrelation (Moran's *I*; metric of clustering) calculated over increasing spatial scales. Gray shaded area represents 95% range of chance values. Positive values indicate clustering of similar values; 0 indicates random spatial organization; negative values indicate spatial segregation of similar values. Gray dashed line indicates the extent of significant clustering. *C*: preferred locations mapped onto array. Preferred location—defined as the location of the peak of the Gaussian model fit to the thresholded activity on an electrode ($R^2 > 0.5$)—was mapped onto the array according to a 2-dimensional spatial color map (*inset*). Gray channels are nontuned; black channels are ground electrodes.

visual field may become less biased toward the contralateral hemifield.

Visual information from the ipsilateral hemifield necessarily crosses the midline via the corpus callosum at some point along the visual processing stream. There is callosal input onto the LPFC from the homotopic area of the opposite hemifield (Goldman-Rakic and Schwartz 1982) as well as sensory and association areas (Barbas et al. 2005). Recent work by Lennert and Martinez-Trujillo (2013) has indicated that ipsilateral and contralateral neurons may play a different role in target selection. The response profiles of the neurons in the same task differ depending on the relevance of the stimulus in the RF. These authors proposed that contralateral neurons seem to be more engaged in target selection, while ipsilateral neurons seem to be more engaged in sustaining attention on a target once it has been selected. However, to fully clarify this issue, one must extend the results of these studies to a variety of tasks and RF mapping methods that go beyond the scope of the present study.

Contrast response functions. It has been suggested that higher-order cortical areas represent more complex stimulus features (Maunsell and Newsome 1987); it is unclear to what extent these areas allocate resources to encode simpler stimulus features, e.g., contrast. In comparison to neurons in early visual areas, the neurons in higher-order areas tend to have a lower semisaturation constant (C_{50}) and thus higher contrast sensitivity. For instance, macaque LGN and V1 neurons have demonstrated a median C_{50} of 0.11–0.5 and 0.33, respectively (Sclar et al. 1990). By contrast, MT neurons display a strikingly lower median C_{50} value of 0.07 (7% contrast normalized to 1.0) (Sclar et al. 1990). Similarly, area 8Ar neurons exhibit a low median C_{50} of 4–6% contrast (present study, Table 1). Although comparisons between studies is difficult because of different methods of measuring luminance contrast and different display features, our results suggest that neurons in area 8Ar have sigmoid contrast response functions and contrast sensitivity similar to neurons in early visual areas.

The distribution of latencies as a function of contrast in our sample also follows a well-described trend (Albrecht et al. 2002) for latencies to be shorter at higher contrast values (Fig. 8). Our results suggest that visually selective neurons in 8Ar inherit their contrast sensitivity from visual neurons.

Topographic organization. An outstanding question is whether RFs of neurons in area 8Ar of the LPFC show a defined topography (e.g., retinotopy). Previous studies have suggested anatomical clustering of neurons with similar re-

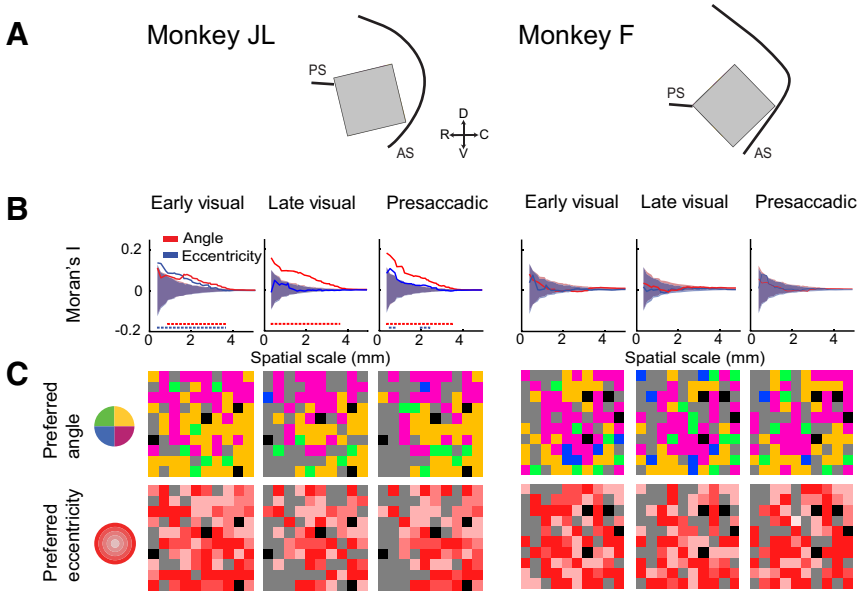

Fig. 10. Anatomical clustering as a function of angle and eccentricity. *A*: schematic illustrating position of array implants. *B*: magnitude of clustering (Moran's *I*) as a function of angle and eccentricity. Dashed lines of each color indicate the extent of significant clustering for each spatial dimension. *C*: preferred angle (*top*) and eccentricity (*bottom*) mapped onto array according to their respective color maps. Gray channels are nontuned; black channels are ground electrodes.

sponse properties (Kiani et al. 2015; Suzuki and Azuma 1983) in the PFC. Indeed, Kiani and colleagues (2015) recorded from microelectrode arrays implanted on the prearcuate convexity in a location very similar to our implantation site. They sampled a number of locations in the visual field and observed RF and MF profiles (Supplemental Fig. S9 in Kiani et al. 2015) similar to those found in the present study (Fig. 5*A*) and conducted a comparison of RF similarity that mirrors our analysis of RF and MF overlap (Fig. 6).

However, differences in recording techniques may render a comparison between previous studies and the present study difficult. In the case of Suzuki and Azuma (1983), the location of penetrations with single electrodes are difficult to analyze since the brain may change in volume during the experiments because of repeated injuries of blood vessels in the region, edema, and dural thickening. In our case, the use of chronically implanted MEAs and intraoperatory pictures allows for a fixed reference system in which the topography of RFs and MFs can be analyzed relative to the position of the neurons on the cortical surface and to fixed landmarks that are visible after dura mater opening (e.g., the arcuate sulcus). Nonetheless, recording with MEAs may also have some limitations, namely, arrays sample neurons from a fixed cortical layer parallel to the array plane, neurons could be sampled twice in different days, and there is a fixed area of 4×4 mm where samples are taken from.

Our results quantitatively demonstrate that groups of neurons with RFs in similar locations were anatomically clustered (Fig. 9*B*), with a slight trend for the upper contralateral visual field to be represented in the ventrolateral portion of the array and the lower contralateral visual field to be represented in the dorsomedial part of the array (Fig. 9*C*). Indeed, these results agree with those of Savaki et al. (2015), who utilized [^{14}C]deoxyglucose quantitative autoradiography to examine activity in the prefrontal cortex of macaques during saccades. Similar to the present investigation, they found a dorsal-to-ventral gradient within area 8Ar representing the contralateral lower to upper visuo-oculomotor space. Taken together, these findings indicate a topographic arrangement of visuo-oculomotor space within area 8Ar.

In the present study, area 8Ar RFs were typically large and eccentric (Fig. 5*A*). This is in concordance with previous reports of neurons in the region between the principal sulcus and the arcuate sulcus (the middle arcuate area) having large, somewhat eccentric RFs (Suzuki and Azuma 1983). Suzuki and Azuma (1983) recorded from the prearcuate cortex spanning from the inferior to the superior limb of the arcuate sulcus and reported a trend for smaller foveal and parafoveal RFs in the inferior portion of the prearcuate cortex, in the approximate location of area 45 (Petrides and Pandya 1999). There is a topographic organization of increasing RF size moving from the inferior toward the middle arcuate area (Suzuki and Azuma 1983). Thus the population of neurons spanning the prearcuate cortex—bounded dorsally by area 8B and ventrally by area 45—likely contains a complete map of eccentricities, and the present study samples from the portion of the map representing an intermediate range of eccentricities (~15 dva).

Although we examined clustering according to eccentricity (Fig. 10*B*), we did not observe the isocontour lines of RF eccentricity reported by Suzuki and Azuma (1983). This could be attributed to the fact that our clustering algorithm was less sensitive to the geometry of a line or the fact that the present study mapped eccentricity out to 15 dva, whereas Suzuki and Azuma (1983) mapped a much larger range of eccentricities (out to 60 dva). Furthermore, Suzuki and Azuma (1983) used *Macaca mulatta* whereas the present study used *Macaca fascicularis*; therefore the different results may be ascribed to species differences.

Although, similar to the FEF, area 8A contains the visual and motor spatial representation of a visual and saccadic target, this area may show functional differences compared with its caudally adjacent neighbor (the FEF). For instance, we find clustering of neurons representing the vector angle of saccades (Fig. 10*B*), whereas in the FEF there is topographic organization of the saccadic amplitude but not angle (Bruce et al. 1985; Stanton et al. 1989). Nevertheless, this finding was only clearly present in one animal; thus this issue needs to be examined in more detail with a larger sample size (number of animals) and homogeneous mapping procedures across areas.

The difference in spatial representation (foveal vs peripheral representation) recapitulates the cytoarchitectonically defined prefrontal areas, although functional borders appear to be gradual. Area 45 receives projections from the inferotemporal cortex area TEO (Webster et al. 1994) representing central vision, whereas medial area 8Ar receives input from the posterior parietal cortex (Yeterian et al. 2012), representing peripheral vision (Motter and Mountcastle 1981; Schall 1995). This trend of central to peripheral, ventrolateral to dorsomedial RF eccentricity in the prearcuate gyrus corresponds to the trend of small-amplitude saccades in ventrolateral portion of the FEF and large-amplitude saccades in the dorsomedial FEF (Bruce et al. 1985).

One interesting finding in our study is that the two neuronal populations of the animals show different tendencies to cluster, at least in respect to the degree of clustering. Clusters of neurons preferring similar location in the visual field seem to be larger and better defined in *monkey JL* compared with *monkey F* (Fig. 9). This difference may be the result of individual variability between animals, e.g., patterns that are intrinsic to each individual according to the interplay between genetically determined connectivity and the effect of environmental stimulation. Alternatively, this variability may be a feature of the prefrontal cortex that is not found in visual areas and may reflect the sole effect of environmental variables on the wiring of the LPFC. Since previous studies have reported that when animals are trained in a motion direction task neurons in area 8Ar are selective for motion direction (Mendoza-Halliday et al. 2014), we tend to support the latter hypothesis (selectivity shaped by learning experience). It is impossible to answer this question with our data; however, the fact that we found such differences in topographic organization between animals opens new questions and hypotheses regarding the role of the prefrontal cortex in individual variability in cognitive skills.

Cells suppressed by visual stimulus at the antipreferred direction. Some visually selective cells in the FEF have been reported to show suppression when a saccade was prepared toward a visual target presented outside the RF (Burman and Segraves 1994), particularly when the target was presented in the hemifield contralateral to that cell's RF (Schall et al. 1995a). Within the LPFC, there have been reports of cells with activity suppressed below baseline in a restricted portion of the

visual field (Mikami et al. 1982). We also characterized a subset of cells with a zone of brisk suppression in the location opposite the zone of activation (Fig. 5*A*), and there was a bias for these suppressed cells to have RF and MF peak activation in the ipsilateral hemifield (Fig. 5*C*).

Recent studies suggest that, during target selection, populations of prefrontal neurons compete or cooperate for preferential processing of a visual stimulus. To this point, during target selection, pairs of FEF neurons with overlapping RFs coordinate by firing in synchrony when a target is placed within the overlapping portion of the RFs. By contrast, neurons with nonoverlapping RFs compete, firing out of synchrony when the target appears in the RF of one neuron but not the other (Cohen et al. 2010). In the present study, suppressed cells tended to have zones of activation in the ipsilateral hemifield (Fig. 5*C*). Some proportion of neurons with contralateral RFs likely suppresses activity of ipsilaterally preferring cells via inhibitory interneurons. These inhibitory circuits may mediate biased competition (Desimone and Duncan 1995) between hemispheres.

Differences and similarities between area 8Ar and FEF. There are a few functional differences in the properties of neurons in area 8Ar reported here and those of neurons in the FEF reported by other studies. It should be noted that many studies of the FEF include recordings spanning both the prearcuate gyrus and the rostral bank of the arcuate sulcus, making it difficult to differentiate the response properties between FEF and 8Ar. Visually responsive cells in the FEF are usually not feature selective, although it has been reported that with training some cells can gain feature selectivity (Bichot et al. 1996). By contrast, neurons in area 8Ar demonstrate feature selectivity in sustained activity during a delayed match-to-sample task (Mendoza-Halliday et al. 2014). Finally, the sensory neurons in the FEF tend to strongly prefer the contralateral visual hemifield (Schall 1991), whereas visually selective neurons in area 8Ar display a greater degree of bilateral representation, with a bias toward the contralateral hemifield (Fig. 5*C*). There appears to be no sharp delineation in response properties in FEF and area 8Ar, but rather a gradient of function moving rostrally.

Considered together, these data suggest that area 8Ar and the FEF may play functionally distinct roles in executive processes involved in the generation of saccades, with the FEF more directly linked to saccade execution. However, the function and connectivity of these two areas are intimately linked; thus they likely work in coordination to select a target for saccades. For example, injection with the retrograde tracer horseradish peroxidase reveals afferent projections to the superior colliculus originating in both the FEF (within the anterior bank of the arcuate sulcus) and area 8Ar (on the prearcuate gyrus) (Fries 1984). One possibility is that area 8Ar is more involved in integrating different types of signals including sensory, reward value, attention, working memory and others, while the FEF is more involved in generating the final gaze command to direct the eyes in space toward objects of interest. The precise mechanism of this process will be addressed by future studies.

Conclusions. Area 8Ar displays visual and saccade-related activity and shares connections with a multitude of visual and oculomotor areas. We found that area 8Ar contains populations of visual, movement, and visuomovement neurons, with RFs and MFs representing both visual hemifields, and that some of the visually selective neurons were modulated by increasing contrast levels. Therefore, we conclude that area 8Ar likely plays a role in visuomotor integration in preparation for saccades. Future studies are necessary to elucidate the mechanism whereby area 8Ar integrates visual information to influence saccade target selection. Although the topographic organization of the LPFC (particularly retinotopy) remains uncertain, we have demonstrated that neurons with similar RF and MF locations are anatomically clustered within an area of 4 × 4 mm of 8Ar, particularly with respect to RF location during the early periods of visual stimulation.

ACKNOWLEDGMENTS

We thank Stephen Nuara and Walter Kucharski for technical support in conducting this experiment. We also thank our laboratory members for their thoughtful critique and comments in preparation of this manuscript.

GRANTS

This work was supported by grants to J. C. Martinez-Trujillo from the Natural Sciences and Engineering Research Council, the EJLB Foundation, the Canadian Institutes of Health Research, and the Canada Research Chair program.

DISCLOSURES

No conflicts of interest, financial or otherwise, are declared by the author(s).

AUTHOR CONTRIBUTIONS

K.R.B. analyzed data; K.R.B. and J.C.M.-T. interpreted results of experiments; K.R.B. prepared figures; K.R.B. drafted manuscript; K.R.B. and J.C.M.-T. edited and revised manuscript; K.R.B., F.P., and J.C.M.-T. approved final version of manuscript; F.P. and A.J.S. performed experiments.

REFERENCES

Albrecht DG, Geisler WS, Frazor RA, Crane AM. Visual cortex neurons of monkeys and cats: temporal dynamics of the contrast response function. *J Neurophysiol* 88: 888–913, 2002.

Albrecht DG, Hamilton DB. Striate cortex of monkey and cat: contrast response function. *J Neurophysiol* 48: 217–237, 1982.

Andersen RA, Asanuma C, Essick G, Siegel RM. Corticocortical connections of anatomically and physiologically defined subdivisions within the inferior parietal lobule. *J Comp Neurol* 296: 65–113, 1990. doi:10.1002/cne.902960106.

Arcaro MJ, Pinsk MA, Li X, Kastner S. Visuotopic organization of macaque posterior parietal cortex: a functional magnetic resonance imaging study. *J Neurosci* 6: 2064–2078, 2011. doi:10.1523/JNEUROSCI.3334-10.2011.

Bahill AT, Clark MR, Stark L. The main sequence, a tool for studying human eye movements. *Math Biosci* 24: 191–204, 1975. doi:10.1016/0025-5564(75)90075-9.

Barbas H, Hilgetag CC, Saha S, Dermon CR, Suski JL. Parallel organization of contralateral and ipsilateral prefrontal cortical projections in the rhesus monkey. *BMC Neurosci* 6: 32, 2005. doi:10.1186/1471-2202-6-32.

Barbas H, Mesulam MM. Organization of afferent input to subdivisions of area 8 in the rhesus monkey. *J Comp Neurol* 200: 407–431, 1981. doi:10.1002/cne.902000309.

Barone P, Joseph JP. Role of the dorsolateral prefrontal cortex in organizing visually guided behavior. *Brain Behav Evol* 33: 132–135, 1989. doi:10.1159/000115915.

Ben Hamed S, Duhamel JR, Bremmer F, Graf W. Representation of the visual field in the lateral intraparietal area of macaque monkeys: a quantitative receptive field analysis. *Exp Brain Res* 140: 127–144, 2001. doi:10.1007/s002210100785.

Bichot NP, Schall JD, Thompson KG. Visual feature selectivity in frontal eye fields induced by experience in mature macaques. *Nature* 381: 697–699, 1996. doi:10.1038/381697a0.

Blatt GJ, Andersen RA, Stoner GR. Visual receptive field organization and cortico-cortical connections of the lateral intraparietal area (area LIP) in the macaque. *J Comp Neurol* 299: 421–445, 1990. doi:10.1002/cne.902990404.

Bruce CJ, Goldberg ME. Primate frontal eye fields. I. Single neurons discharging before saccades. *J Neurophysiol* 53: 603–635, 1985.

Bruce CJ, Goldberg ME, Bushnell MC, Stanton GB. Primate frontal eye fields. II. Physiological and anatomical correlates of electrically evoked eye movements. *J Neurophysiol* 54: 714–734, 1985.

Burman DD, Segraves MA. Primate frontal eye field activity during natural scanning eye movements. *J Neurophysiol* 71: 1266–1271, 1994.

Cohen JY, Crowder EA, Heitz RP, Subraveti CR, Thompson KG, Woodman GF, Schall JD. Cooperation and competition among frontal eye field neurons during visual target selection. *J Neurosci* 30: 3227–3238, 2010. doi:10.1523/JNEUROSCI.4600-09.2010.

Desimone R, Duncan J. Neural mechanisms of selective visual attention. *Annu Rev Neurosci* 18: 193–222, 1995. doi:10.1146/annurev.ne.18.030195.001205.

Dow BM, Snyder AZ, Vautin RG, Bauer R. Magnification factor and receptive field size in foveal striate cortex of the monkey. *Exp Brain Res* 44: 213–228, 1981. doi:10.1007/BF00237343.

Everling S, Tinsley CJ, Gaffan D, Duncan J. Filtering of neural signals by focused attention in the monkey prefrontal cortex. *Nat Neurosci* 5: 671–676, 2002. doi:10.1038/nn874.

Felleman DJ, Van Essen DC. Distributed hierarchical processing in the primate cerebral cortex. *Cereb Cortex* 1: 1–47, 1991. doi:10.1093/cercor/1.1.1.

Fries W. Cortical projections to the superior colliculus in the macaque monkey: a retrograde study using horseradish peroxidase. *J Comp Neurol* 230: 55–76, 1984. doi:10.1002/cne.902300106.

Funahashi S, Bruce CJ, Goldman-Rakic PS. Neuronal activity related to saccadic eye movements in the monkey's dorsolateral prefrontal cortex. *J Neurophysiol* 65: 1464–1483, 1991.

Gattass R, Sousa AP, Gross CG. Visuotopic organization and extent of V3 and V4 of the macaque. *J Neurosci* 8: 1831–1845, 1988.

Genovesio A, Brasted PJ, Mitz AR, Wise SP. Prefrontal cortex activity related to abstract response strategies. *Neuron* 47: 307–320, 2005. doi:10.1016/j.neuron.2005.06.006.

Goldman-Rakic PS, Schwartz ML. Interdigitation of contralateral and ipsilateral columnar projections to frontal association cortex in primates. *Science* 216: 755–757, 1982. doi:10.1126/science.6177037.

Hair JF, Sarstedt M, Ringle CM, Mena JA. An assessment of the use of partial least squares structural equation modeling in marketing. *J Acad Mark Sci* 40: 414–433, 2012. doi:10.1007/s11747-011-0261-6.

Hanes DP, Thompson KG, Schall JD. Relationship of presaccadic activity in frontal eye field and supplementary eye field to saccade initiation in macaque: Poisson spike train analysis. *Exp Brain Res* 103: 85–96, 1995. doi:10.1007/BF00241967.

Hubel DH, Wiesel TN. Receptive fields and functional architecture of monkey striate cortex. *J Physiol* 195: 215–243, 1968. doi:10.1113/jphysiol.1968.sp008455.

Hubel DH, Wiesel TN. Uniformity of monkey striate cortex: a parallel relationship between field size, scatter, and magnification factor. *J Comp Neurol* 158: 295–305, 1974. doi:10.1002/cne.901580305.

Khayat PS, Niebergall R, Martinez-Trujillo JC. Attention differentially modulates similar neuronal responses evoked by varying contrast and direction stimuli in area MT. *J Neurosci* 30: 2188–2197, 2010. doi:10.1523/JNEUROSCI.5314-09.2010.

Kiani R, Cueva CJ, Reppas JB, Newsome WT. Dynamics of neural population responses in prefrontal cortex indicate changes of mind on single trials. *Curr Biol* 24: 1542–1547, 2014. doi:10.1016/j.cub.2014.05.049.

Kiani R, Cueva CJ, Reppas JB, Peixoto D, Ryu SI, Newsome WT. Natural grouping of neural responses reveals spatially segregated clusters in prearcuate cortex. *Neuron* 85: 1359–1373, 2015. doi:10.1016/j.neuron.2015.02.014.

Kowler E, Blaser E. The accuracy and precision of saccades to small and large targets. *Vision Res* 35: 1741–1754, 1995. doi:10.1016/0042-6989(94)00255-K.

Leavitt ML, Pieper F, Sachs A, Joober R, Martinez-Trujillo JC. Structure of spike count correlations reveals functional interactions between neurons in dorsolateral prefrontal cortex area 8a of behaving primates. *PLoS One* 8: e61503, 2013. doi:10.1371/journal.pone.0061503.

Legéndy CR, Salcman M. Bursts and recurrences of bursts in the spike trains of spontaneously active striate cortex neurons. *J Neurophysiol* 53: 926–939, 1985.

Lennert T, Martinez-Trujillo J. Strength of response suppression to distracter stimuli determines attentional-filtering performance in primate prefrontal neurons. *Neuron* 70: 141–152, 2011. doi:10.1016/j.neuron.2011.02.041.

Lennert T, Martinez-Trujillo JC. Prefrontal neurons of opposite spatial preference display distinct target selection dynamics. *J Neurosci* 33: 9520–9529, 2013. doi:10.1523/JNEUROSCI.5156-12.2013.

Martínez-Trujillo J, Treue S. Attentional modulation strength in cortical area MT depends on stimulus contrast. *Neuron* 35: 365–370, 2002. doi:10.1016/S0896-6273(02)00778-X.

Maunsell JH, van Essen DC. The connections of the middle temporal visual area (MT) and their relationship to a cortical hierarchy in the macaque monkey. *J Neurosci* 3: 2563–2586, 1983.

Maunsell JH, Newsome WT. Visual processing in monkey extrastriate cortex. *Annu Rev Neurosci* 10: 363–401, 1987. doi:10.1146/annurev.ne.10.030187.002051.

Maynard EM, Nordhausen CT, Normann RA. The Utah Intracortical Electrode Array: a recording structure for potential brain-computer interfaces. *Electroencephalogr Clin Neurophysiol* 102: 228–239, 1997. doi:10.1016/S0013-4694(96)95176-0.

Mendoza-Halliday D, Torres S, Martinez-Trujillo JC. Sharp emergence of feature-selective sustained activity along the dorsal visual pathway. *Nat Neurosci* 17: 1255–1262, 2014. doi:10.1038/nn.3785.

Michelson AA. *Studies in Optics*. Chicago, IL: Univ. of Chicago Press, 1927.

Mikami A, Ito S, Kubota K. Visual response properties of dorsolateral prefrontal neurons during visual fixation task. *J Neurophysiol* 47: 593–605, 1982.

Miller EK. The prefrontal cortex: complex neural properties for complex behavior. *Neuron* 22: 15–17, 1999. doi:10.1016/S0896-6273(00)80673-X.

Moran PA. Notes on continuous stochastic phenomena. *Biometrika* 37: 17–23, 1950. doi:10.1093/biomet/37.1-2.17.

Motter BC, Mountcastle VB. The functional properties of the light-sensitive neurons of the posterior parietal cortex studied in waking monkeys: foveal sparing and opponent vector organization. *J Neurosci* 1: 3–26, 1981.

Normann RA, Maynard EM, Rousche PJ, Warren DJ. A neural interface for a cortical vision prosthesis. *Vision Res* 39: 2577–2587, 1999. doi:10.1016/S0042-6989(99)00040-1.

Patel GH, Shulman GL, Baker JT, Akbudak E, Snyder AZ, Snyder LH, Corbetta M. Topographic organization of macaque area LIP. *Proc Natl Acad Sci USA* 107: 4728–4733, 2010. doi:10.1073/pnas.0908092107.

Petrides M, Pandya DN. Dorsolateral prefrontal cortex: comparative cytoarchitectonic analysis in the human and the macaque brain and corticocortical connection patterns. *Eur J Neurosci* 11: 1011–1036, 1999. doi:10.1046/j.1460-9568.1999.00518.x.

Preuss TM, Goldman-Rakic PS. Myelo- and cytoarchitecture of the granular frontal cortex and surrounding regions in the strepsirhine primate *Galago* and the anthropoid primate *Macaca*. *J Comp Neurol* 310: 429–474, 1991. doi:10.1002/cne.903100402.

Rossi AF, Bichot NP, Desimone R, Ungerleider LG. Top down attentional deficits in macaques with lesions of lateral prefrontal cortex. *J Neurosci* 27: 11306–11314, 2007. doi:10.1523/JNEUROSCI.2939-07.2007.

Savaki HE, Gregoriou GG, Bakola S, Moschovakis AK. Topography of visuomotor parameters in the frontal and premotor eye fields. *Cereb Cortex* 25: 3095–3106, 2015. doi:10.1093/cercor/bhu106.

Schall JD. Neuronal activity related to visually guided saccades in the frontal eye fields of rhesus monkeys: comparison with supplementary eye fields. *J Neurophysiol* 66: 559–579, 1991.

Schall JD. Neural basis of saccade target selection. *Rev Neurosci* 6: 63–85, 1995. doi:10.1515/REVNEURO.1995.6.1.63.

Schall JD, Hanes DP, Thompson KG, King DJ. Saccade target selection in frontal eye field of macaque. I. Visual and premovement activation. *J Neurosci* 15: 6905–6918, 1995a.

Schall JD, Morel A, King DJ, Bullier J. Topography of visual cortex connections with frontal eye field in macaque: convergence and segregation of processing streams. *J Neurosci* 15: 4464–4487, 1995b.

Schlag J, Schlag-Rey M. Evidence for a supplementary eye field. *J Neurophysiol* 57: 179–200, 1987.

Sclar G, Maunsell JH, Lennie P. Coding of image contrast in central visual pathways of the macaque monkey. *Vision Res* 30: 1–10, 1990. doi:10.1016/0042-6989(90)90123-3.

Seo H, Barraclough DJ, Lee D. Dynamic signals related to choices and outcomes in the dorsolateral prefrontal cortex. *Cereb Cortex* 17, *Suppl* 1: i110–i117, 2007. doi:10.1093/cercor/bhm064.

Sparks DL, Holland R, Guthrie BL. Size and distribution of movement fields in the monkey superior colliculus. *Brain Res* 113: 21–34, 1976. doi:10.1016/0006-8993(76)90003-2.

Sparks DL, Mays LE. Movement fields of saccade-related burst neurons in the monkey superior colliculus. *Brain Res* 190: 39–50, 1980. doi:10.1016/0006-8993(80)91158-0.

Spillmann L, Ransom-Hogg A, Oehler R. A comparison of perceptive and receptive fields in man and monkey. *Hum Neurobiol* 6: 51–62, 1987.

Stanton GB, Bruce CJ, Goldberg ME. Topography of projections to the frontal lobe from the macaque frontal eye fields. *J Comp Neurol* 330: 286–301, 1993. doi:10.1002/cne.903300209.

Stanton GB, Deng SY, Goldberg ME, McMullen NT. Cytoarchitectural characteristic of the frontal eye fields in macaque monkeys. *J Comp Neurol* 282: 415–427, 1989. doi:10.1002/cne.902820308.

Suzuki H, Azuma M. Topographic studies on visual neurons in the dorsolateral prefrontal cortex of the monkey. *Exp Brain Res* 53: 47–58, 1983. doi:10.1007/BF00239397.

Takeda K, Funahashi S. Prefrontal task-related activity representing visual cue location or saccade direction in spatial working memory tasks. *J Neurophysiol* 87: 567–588, 2002.

Tolias AS, Moore T, Smirnakis SM, Tehovnik EJ, Siapas AG, Schiller PH. Eye movements modulate visual receptive fields of V4 neurons. *Neuron* 29: 757–767, 2001. doi:10.1016/S0896-6273(01)00250-1.

Tremblay S, Pieper F, Sachs A, Martinez-Trujillo J. Attentional filtering of visual information by neuronal ensembles in the primate lateral prefrontal cortex. *Neuron* 85: 202–215, 2015. doi:10.1016/j.neuron.2014.11.021.

Ungerleider LG, Desimone R. Cortical connections of visual area MT in the macaque. *J Comp Neurol* 248: 190–222, 1986. doi:10.1002/cne.902480204.

Van Essen DC, Maunsell JH, Bixby JL. The middle temporal visual area in the macaque: myeloarchitecture, connections, functional properties and topographic organization. *J Comp Neurol* 199: 293–326, 1981. doi:10.1002/cne.901990302.

Van Essen DC, Newsome WT, Maunsell JH. The visual field representation in striate cortex of the macaque monkey: asymmetries, anisotropies, and individual variability. *Vision Res* 24: 429–448, 1984. doi:10.1016/0042-6989(84)90041-5.

Wallis JD, Anderson KC, Miller EK. Single neurons in prefrontal cortex encode abstract rules. *Nature* 411: 953–956, 2001. doi:10.1038/35082081.

Webster MJ, Bachevalier J, Ungerleider LG. Connections of inferior temporal areas TEO and TE with parietal and frontal cortex in macaque monkeys. *Cereb Cortex* 4: 470–483, 1994. doi:10.1093/cercor/4.5.470.

Wegener SP, Johnston K, Everling S. Microstimulation of monkey dorsolateral prefrontal cortex impairs antisaccade performance. *Exp Brain Res* 190: 463–473, 2008. doi:10.1007/s00221-008-1488-4.

Wise SP, Murray EA, Gerfen CR. The frontal cortex-basal ganglia system in primates. *Crit Rev Neurobiol* 10: 317–356, 1996. doi:10.1615/CritRevNeurobiol.v10.i3-4.30.

Womelsdorf T, Anton-Erxleben K, Treue S. Receptive field shift and shrinkage in macaque middle temporal area through attentional gain modulation. *J Neurosci* 28: 8934–8944, 2008. doi:10.1523/JNEUROSCI.4030-07.2008.

Yeterian EH, Pandya DN, Tomaiuolo F, Petrides M. The cortical connectivity of the prefrontal cortex in the monkey brain. *Cortex* 48: 58–81, 2012. doi:10.1016/j.cortex.2011.03.004.

Zuur AF, Ieno EN, Smith GM. *Analyzing Ecological Data*. New York: Springer, 2007.